STRUCTURAL
BIOLOGY

Volume 76 (2020)

Supporting information for article:

Crystal and solution structures of fragments of the human leucocyte common antigen-related protein

Joachim Vilstrup, Amanda Simonsen, Thea Birkefeldt, Dorthe Strandbygård, Jeppe Lyngsø, Jan Skov Pedersen and Søren Thirup

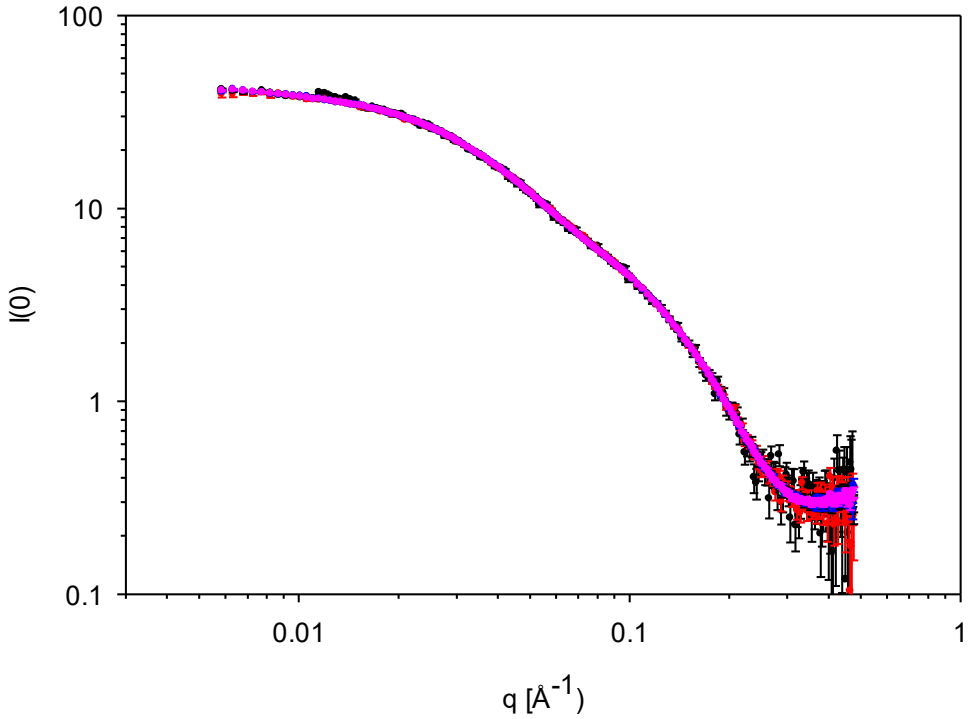

Figure S1 . SAXS data for all concentrations. Concentrations are 1.07 (black points), 2.25 (red), 5.65 (green), 7.8 (yellow), 8.4 (blue), and 11.7 mg/mL (magenta). The individual data sets are difficult to distinguish in the plot due to close overlap.

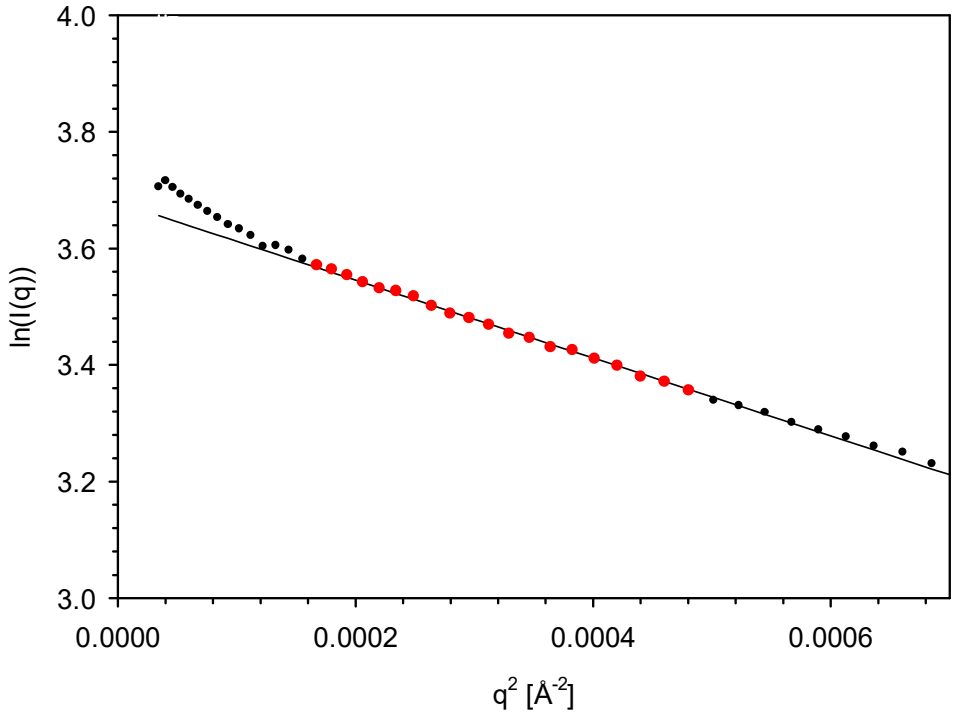

Figure S2 Guinier plot and fit. Only the red filled points were used in the fit.

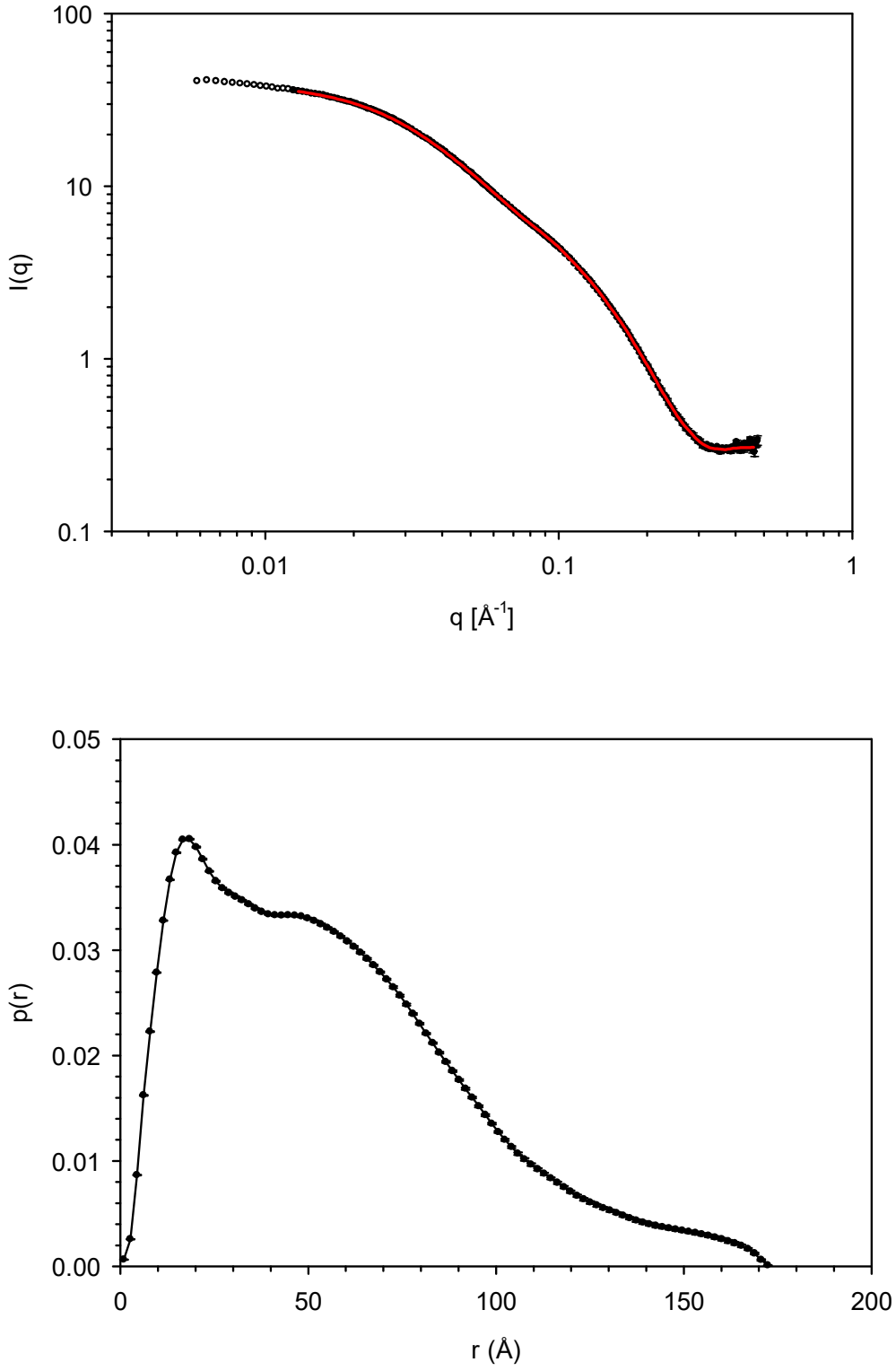

Figure S3 Fit to the high concentration data by IFT for $q > 0.0125$ Å^{-1} and the corresponding $p(r)$ function.

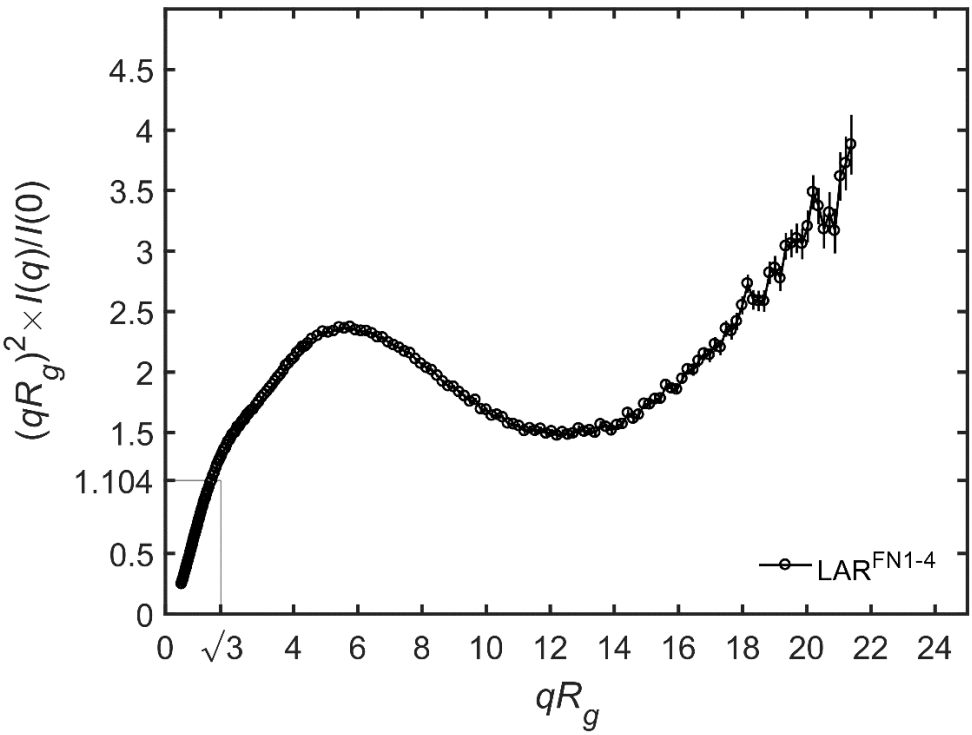

Figure S4 Normalized Kratky plot of the high concentration data.

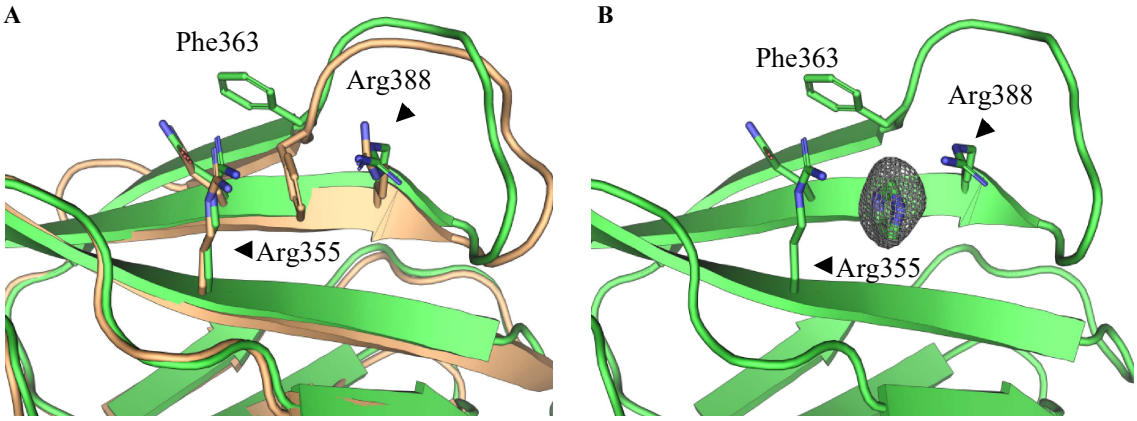

Figure S5 A: Superposition of the two LAR^{FN1-2} monomers. In one monomer Phe363 is sandwiched between Arg355 and Arg388. This switch induces a slight shift in the surrounding loop. B: Instead of the aromatic side chain from Phe363 an imidazole molecule was found sandwiched between Arg355 and Arg388. The difference density shown is a *Fo-Fc* map calculated omitting the imidazole molecule and contoured at 3.0 σ

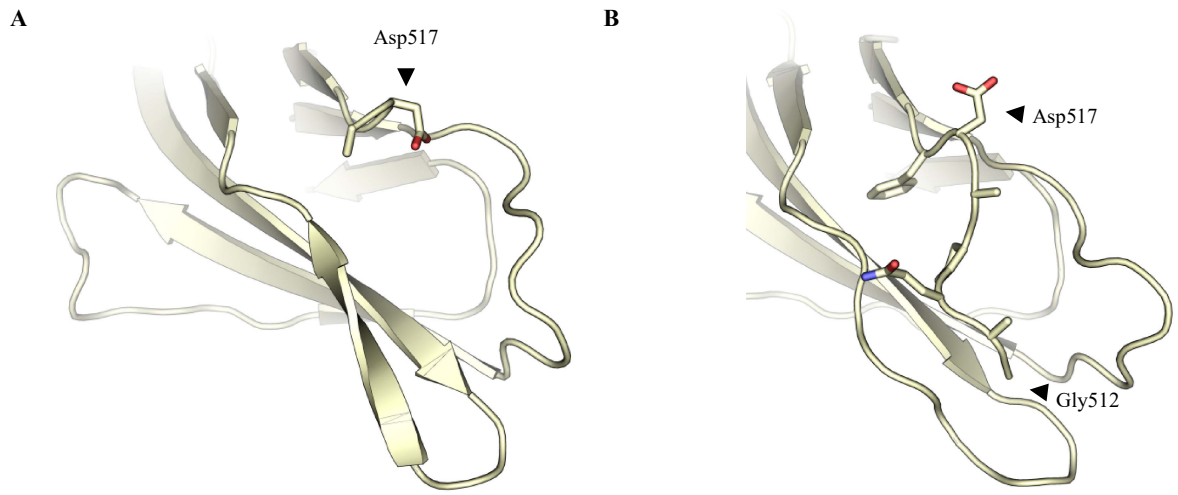

Figure S6 FNIII domain three from LAR^{FN3-4} from the two monomers in the asymmetric unit. In one monomer the N-terminal residues (Gly512 through Asp517) are flipped out and results in the formation of an additional β-strand.

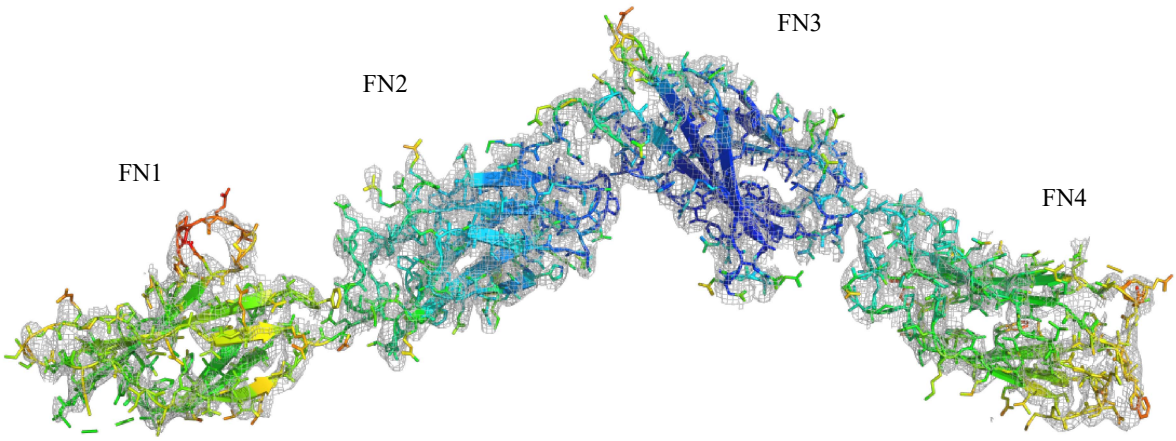

Figure S7 Crystal structure of LAR^{FN1-4} overlaid with $2F_o$-F_C electron density map contoured at 1.5 σ. LAR^{FN1-4} is shown as cartoon and coloured according to *B* factors, i.e. blue indicates lowest *B* factor and red highest.

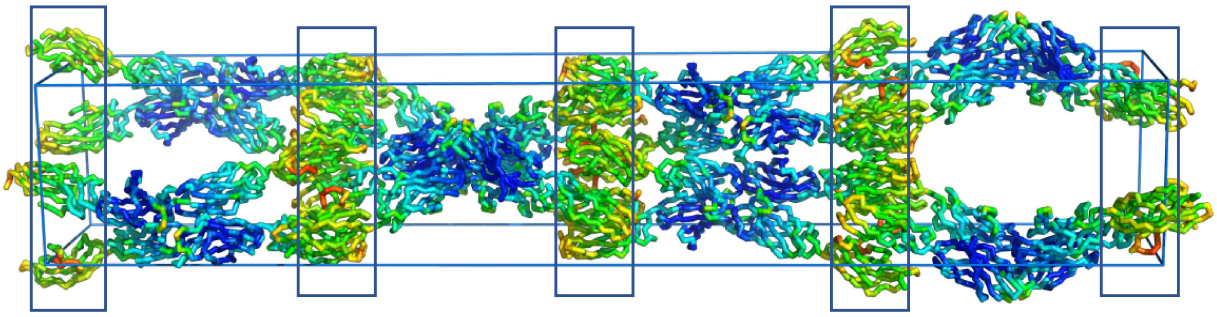

Figure S8 Crystallographic unit cell with the *b* axis extending perpendicular to the plane of the image. LAR^{FN1-4} main chain is shown as tube with radius proportional to the *B* factor and coloured according to *B* factor, i.e. blue indicates lowest *B* factor and red highest.

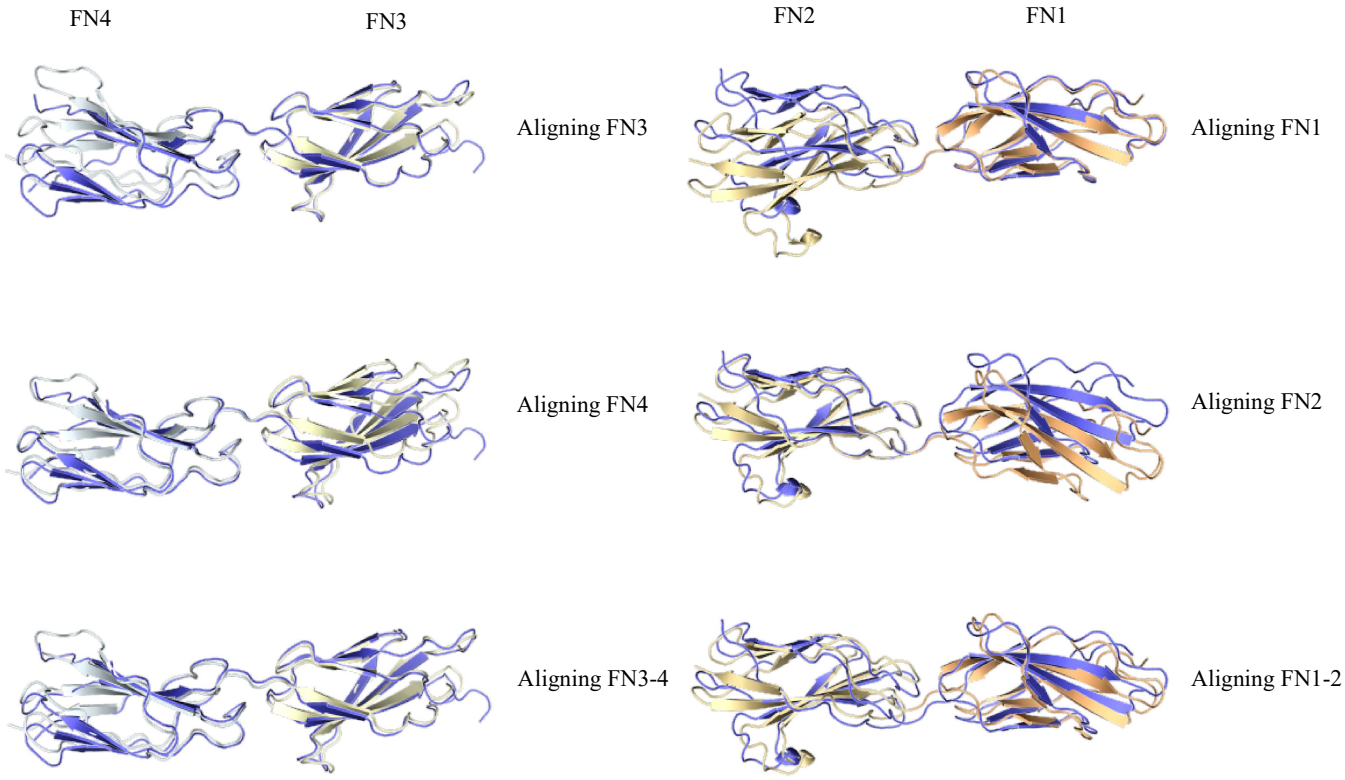

Figure S9 Structural flexibility is found between FNIII domains. Superimposing the individual FNIII domains for the high-resolution structures onto the crystal structure of LAR^{FN1-4}.

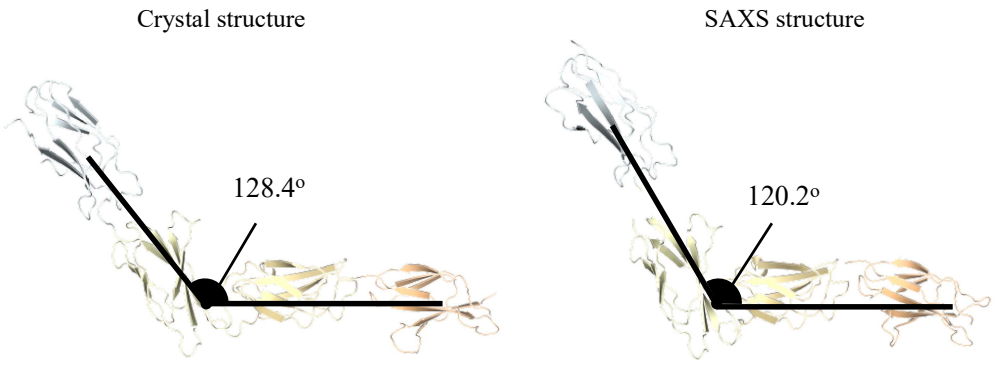

Figure S10 Comparison of the crystal structure and the most probable SAXS model. A difference of 8.2° was observed in the hinge region.

Table S1 Cloning, expression and peptide sequence for LAR^{FN1-2}. His-tag and TEV site are underlined in the peptide sequence.

Sample	LAR^{FN1-2}
Source organism	*H. sapiens*
DNA source	Generated from LAR^{FN1-4}
Forward primer	5'-GTATTTCCAAGGCGCGCAGCCGGCGG-3'
Reverse primer	5'-CCGCCGGCTGCGCGCCTTGGAAATAC-3'
Expression vector	pET9a
Expression host	*E. coli* BL21(DE3)
Complete amino acid sequence of the construct produced	MHHHHHHENLYFQGKPPIDLVVTETTATSVTLTWDSGNSEPVTYYGIQYR AAGTEGPFQEVDGVATTRYSIGGLSPFSEYAFRVLAVNSIGRGPPSEAVR ARTGEQAPSSPPRRVQARMLSASTMLVQWEPPEEPNGLVRGYRVYYTPDS RRPPNAWHKHNTDAGLLTTVGSLLPGITYSLRVLAFTAVGDGPPSPTIQV KTQQGVP

Table S2 Cloning, expression and peptide sequence for LAR^{FN3-4}. His-tag and TEV site are underlined in the peptide sequence.

Sample	LAR^{FN3-4}
Source organism	*H. sapiens*
DNA source	Generated from LAR^{FN1-4}
Forward primer	5'-CCAACAAGGCGTTCCGTAACTCGAGGGATCCG-3'
Reverse primer	5'-CGGATCCCTCGAGTTACGGAACGCCTTGTTGG-3'
Expression vector	pET9a
Expression host	*E. coli*
Complete amino acid sequence of the construct produced	MHHHHHHENLYFQGAQPADFQAEVESDTRIQLSWLLPPQERIIMYELVYW AAEDEDQQHKVTFDPTSSYTLEDLKPDTLYRFQLAARSDMGVGVFTPTIEA RTAQSTPSAPPQKVMCVSMGSTTVRVSWVPPPADSRNGVITQYSVAYEAV DGEDRGRHVVDGISREHSSWDLVGLEKWTEYRVWVRAHTDVGPGPESSPV LVRTDED

Table S3 Cloning, expression and peptide sequence for LAR^{FN1-4}. His-tag and TEV site are underlined in the peptide sequence.

Sample	LAR^{FN1-4}
Source organism	H. sapiens
DNA source	Synthetic
Expression vector	pET9a
Expression host	E. Coli BL21 (DE3)
Complete amino acid sequence of the construct produced	MHHHHHHENLYFQGPKPPIDLVVTETTATSVTLTWDSGNSEPVTYYGIQY RAAGTEGPFQEVDGVATTRYSIGGLSPFSEYAFRVLAVNSIGRGPPSEAV RARTGEQAPSSPPRRVQARMLSASTMLVQWEPPEEPNGLVRGYRVYYTPD SRRPPNAWHKHNTDAGLLTTVGSLLPGITYSLRVLAFTAVGDGPPSPTIQ VKTQQGVPAQPADFQAEVESDTRIQLSWLLPPQERIIMYELVYWAAEDED QQHKVTFDPTSSYTLEDLKPDTLYRFQLAARSDMGVGVFTPTIEARTAQS TPSAPPQKVMCVSMGSTTVRVSWVPPPADSRNGVITQYSVAYEAVDGEDR GRHVVDGISREHSSWDLVGLEKWTEYRVWVRAHTDVGPGPESSPVLVRTD ED

Table S4 Cloning, expression and peptide sequence for LAR^{Ig1-3}. Gp67 signal sequence, His-tag and TEV site are underlined in the peptide sequence.

Sample	LAR^{Ig1-3}
Source organism	H. sapiens
Forward primer	5' -AGGTACCCCTGTCTTCATTAAAGTCCCTG -3'
Reverse primer	5'- AGAATTCTCAAGCTTTCACTGTGACCTGGG -3
Cloning vector	pOET2
Expression vector	FlashBAC virus
Expression host	Spodoptera frugiperda (sf9) insect cells
Complete amino acid sequence of the construct produced	MVSAIVLYVLLAAAAHSAFAHHHHHHENLYFQGTPVFIKVPEDQTGLSGG VASFVCQATGEPKPRITWMKKGKKVSSQRFEVIEFDDGAGSVLRIQPLRV QRDEAIYECTATNSLGEINTSAKLSVLEEEQLPPGFPSIDMGPQLKVVEK ARTATMLCAAGGNPDPEISWFKDFLPVDPATSNGRIKQLRSGALQIESSE ESDQGKYECVATNSAGTRYSAPANLYVRVRRVAPRFSIPPSSQEVMPGGS VNLTCVAVGAPMPYVKWMMGAEELTKEDEMPVGRNVLELSNVVRSANYTC VAISSLGMIEATAQVTVKA

Table S5 Cloning, expression and peptide sequence for LAR^{FN5-8}. His-tag and TEV site is underlined are the peptide sequence.

Sample	LAR^{FN5-8}
Source organism	*H. sapiens*
DNA source	pOET2
Forward primer	TATTCATATGCACCCACCACCATCAC
Reverse primer	ATTAAGGATCCAAGCTTCTAGAGTCGAC
Expression vector	pET9a
Expression host	*E. coli*
Complete amino acid sequence of the construct produced	MHHHHHHENLYFQGTPPRKVEVEPLNSTAVHVYWKLPVPSKQHGQIRGYQ VTYVRLENGEPRGLPIIQDVMLAEAQETTISGLTPETTYSVTVAAYTTKG DGARSKPKIVTTTGAVPGRPTMMISTTAMNTALLQWHPPKELPGELLGYR LQYCRADEARPNTIDFGKDDQHFTVTGLHKGTTYIFRLAAKNRAGLGEEF EKEIRTPEDLPSGFPQNLHVTGLTTSTTELAWDPPVLAERNGRIISYTVV FRDINSQQELQNITTDTRFTLTGLKPDTTYDIKVRAWTSKGSGPLSPSIQ SRTMPVEQVFAKNFRVAAAMKTSVLLSWEVPDSYKSAVPFKILYNGQSVE VDGHSMRKLIADLQPNTEYSFVLMNRGSSAGGLQHLVSIRTAPD

Table S6 Rigid-body refinement. Model 5 is the most probable model as it has the lowest average normalized spatial discrepancy (Teslovich *et al*., 2010) to the other models

Structure	χ2 for model	Rg [Å]	Dmax [Å]	Average NSD to all other models	NSD to Model 5
Original	85.6	46.89	181.39	1.94	1.59
Model 1	4.1	44.77	176.79	1.06	0.85
Model 2	3.7	45.06	175.92	1.28	1.01
Model 3	4.3	44.10	171.62	1.46	1.05
Model 4	4.0	45.13	176.02	1.07	1.32
Model 5*	3.9	44.68	175.68	1.05	0.00
Model 6	3.9	44.83	176.53	1.24	0.70
Model 7	3.9	44.83	173.49	1.20	1.16
Model 8	3.9	44.62	174.42	1.12	0.19
Model 9	3.9	44.79	177.42	1.27	0.88
Model 10	3.9	44.55	173.89	1.13	1.07
Average model 1-10		44.93 ± 0.21	175.74 ± 0.76		

Table S7 Analysis of interdomain flexibility. Superposition of Cα atoms from LAR fragments. E.g. in the top row FNIII domain one from LAR^{FN1-2} was superimposed with FNIII domain one from LAR^{FN1-4}.

		LAR^{FN1-4}					
	r.m.s.d / Å	FN1	FN2	FN1-2	FN3	FN4	FN3-4
	FN1	0.62					
LAR^{FN1-2}	FN2		0.298				
	FN1-2			1.922			
	FN3				0.422		
LAR^{FN3-4}	FN4					0.802	
	FN3-4						0.944